あるBlissは，振動変位及び周波数特性について記しているが[12],[13]，周波数が高くなるにつれて変位が徐々に増大するなど，実験条件なども含めてあいまいな点が多い．

そこで今回，オプタコンの駆動周波数と駆動電圧を変化させ，触知ピンに指を押しあてた状況下での触知ピンの挙動を，レーザ変位計を使って精密に計測し，その変位と周波数との関係を求めた．本論文ではその結果を紹介し，触覚の基本である機械受容ユニットの特性を踏まえた考察を行う．

2. 触知覚の機序

軽微な振動刺激が皮膚に与えられたとき，ヒトがその存在を知覚できる最小の変位は，振動周波数に依存して変化する．それが振動検出しきい曲線である．Bolanowskiらは巧妙な心理物理実験により，その曲線の背後に四つの異なる振動検出チャネルが存在することを示し，それぞれNP（Non Pacinian）I，NP II，NP III，及びP（Pacinian）チャネルとした[14]．このうちPチャネルでのみプローブ先端の面積が大きくなるにつれて，しきい値が下がることをGescheiderらが示している[15]．以上をまとめて図1に示す．なお，縦軸は原図に倣い1.0 μmピークの振幅を基準にして，それよりどのくらいの変位を加えれば振動を感じるかを，横軸の各振動周波数に対してdBでしきい値として表している．

一方，神経生理分野では，皮膚内に分布していて皮膚への機械刺激を受容する受容器と，それらを終末とする求心性神経繊維とを一くくりにして，機械受容ユニットと呼ぶことが多い．Johanssonらは，微小電図法による機械受容ユニットの活動記録から，受容野と順応性を手掛りに，FA (Fast Adaptation)–I及びFA–II，SA (Slowly Adaptation)–I及びSA–IIの主要な四つの型を確定した[16]．実は上述のNP–IがFA–I，NP–IIがSA–II，NP–IIIがSA–I，そしてPチャネルがFA–IIに対応することが知られている．以降はJohanssonの用語を用いることにする．表1に，機械受容ユニットの特性を対比して示す．

Johnsonらによる一連の研究で，次に示すような四つの機械受容ユニットの神経機序が明らかにされた．

（1） SA–Iは四つの機械受容ユニットの中で受容野は最も小さい．また一様な背景を抑制して空間の微細な変化を強調する機能がある[17]．この機能によりSA–Iは空間分解能を支配している．

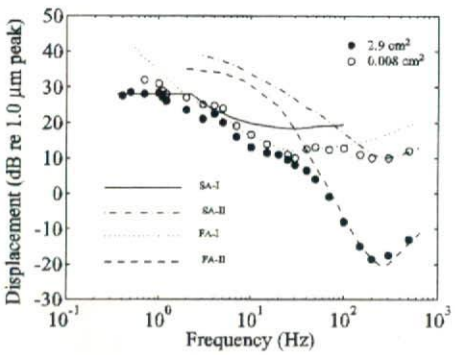

図1　振動検出しきい曲線の拡張周波数範囲を適用した4チャネルモデル（文献[14],[15]より作成）

Fig. 1　Four-channel model of mechanoreception with extended frequency ranges of the tuning curves of the P channels. (Adopted from [14], [15])

表1　機械受容器の種類と特徴

Table 1　Type and characteristics of mechanoreceptor.

	受容器	受容野 (mm^2)	神経支配密度 (本/cm^2)	深さ
SA–I	Merkel	11	60	浅い
SA–II	Ruffine	59	10	深い
FA–I	Meissner	13	140	浅い
FA–II	Pacini	101	20	深い

（2） SA–IIは刺激の方向に対して感受性をもつ．

（3） FA–IはSA–Iが空間分解能に優れるのに対して，皮膚表面での滑りや負荷の急激な変化を検出する．

（4） FA–IIは最も感度の高い機械受容ユニットであり振動刺激において高い感度をもつ．

ちなみに，オプタコンは視覚代行器としての用途が主であり，その場合その駆動周波数が230 Hzで固定されている．これは開発者らによると，指先で毎分100ワードを読解するための指先に与える情報量から計算したものとしている[18]．つまり指先でなぞりながら文字を読解するためには，なぞり速度が速くなるほど触提示パターン変更頻度を上げねばならないことによる．これを図1の振動検出しきい曲線からすると，FA–IIが最も感度の高い領域となる．そして，最も空間分解能の高い機械受容ユニットであるSA–Iは，触知覚にほとんど関与していないことになる．この点に関しては**6.**で触れる．

3. 計測方法

指と接触している状態下での触知ピンの変位は，

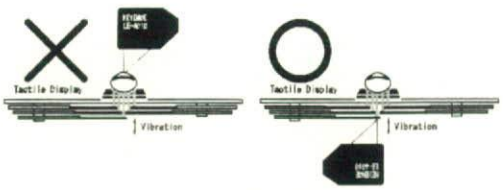

図 2 計測方法
Fig. 2 Measurement method.

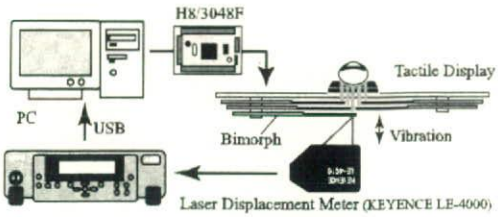

図 3 システム構成
Fig. 3 System configuration.

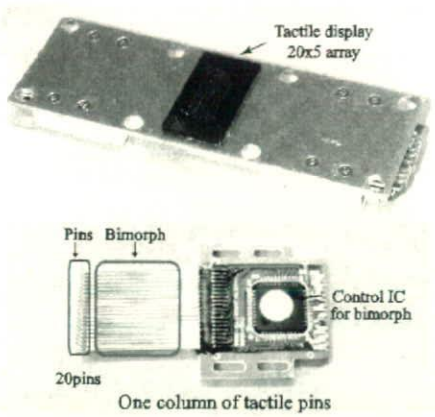

図 4 触知ピンモジュール
Fig. 4 Tactile pin modules.

1960 年代後半の Bliss らの計測例があるのみで，触覚情報処理機能研究の触刺激ツールとしては基本特性の資料が不足している．そこで本研究では，(1) 指と接触状態にある触知ピンの変位を精密に計測し，その変位と周波数特性を求め，(2) 得られた資料を触知覚の基盤となる機械受容ユニットの特性に当てはめて，オプタコン-II の機械特性を評価する．

まず，本研究では評価の基礎となる触知ピンの変位計測を行うが，問題となるのはその計測方法である．指と接触状態にある触知ピンは，接触しているがゆえに指によってその頂点が隠されてしまい，変位を計測することが難しい．したがって，本研究では図 2 のように触覚提示装置の下部から，触知ピンを駆動しているバイモルフ素子の変位を計測する．このとき，接触式の測距センサで計測を行うと触知ピンに応力がかかり正確な変位が計測できないため，レーザ式測距センサを用いて非接触での計測を行う．以上の方法により，指と接触・非接触の状況下での触知ピンの変位計測を行う．

3.1 実験装置

実験装置のシステム全体構成を図 3 に示す．システムはパソコン (PC)，マイクロコンピュータ，オプタコン-II の触知ピンアレー，レーザ変位計から構成される．本研究ではオプタコン-II の触知ピンアレーを触覚提示装置とする．PC は，触覚提示装置で提示する触知ピンの駆動周波数の設定とレーザ変位計からのデータ記録に使用する．マイクロコンピュータは H8/3048F を使用し，PC から指令された駆動振動数に応じた制御信号を触覚提示装置に送る．

以下に，それぞれの実験装置について詳説する．

3.1.1 オプタコン-II

読書材料の上をカメラで走査すると，カメラで取り込んだ映像の文字部分に相当する触知ピンアレーの箇所が振動し，指先に形状情報を伝える．形状情報のまま取り扱うので，図形の読取りにも応用できる．カメラで撮影できるものであれば触覚イメージに変換できるため，文書を読む必要のあるあらゆる場面で利用された．

本研究では第二世代のオプタコンであるオプタコン-II の触知ピンアレーを触覚提示部として用いた．第一世代のオプタコンと比較すると小型化と軽量化が図られ，触知ピンの本数や配置が変更になっているが，両者において 230 Hz の駆動周波数で用いることは共通であり，本研究で目的とする指接触下での触知ピンの変位計測は行われていない．図 4 に触覚提示装置と，その構成要素である触知ピンモジュールを示す．それぞれのピンはバイモルフ型圧電アクチュエータ（図 5）によって駆動しており，アクチュエータの寸法は長さ 37.0 mm × 幅 1.05 mm × 厚み 0.55 mm，駆動電圧は公称 50 V である．

圧電アクチュエータは電界により伸縮するため，分極方向を逆にした 2 枚の圧電素子を張り合わせ，一方を長手方向に伸ばし，もう一方を縮めることにより屈曲させ，変位や力を得ることができる．この変位は印加する電圧で制御することができることから，オプタコン-II には刺激強度調節つまみとして可変抵抗が装

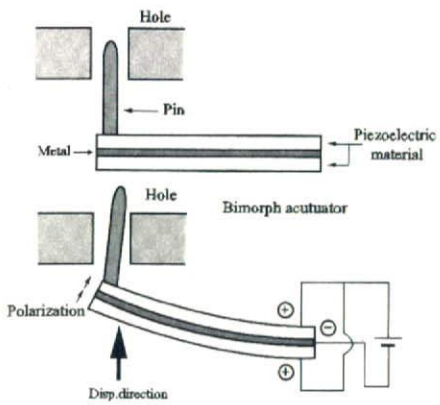

図 5　バイモルフ型圧電アクチュエータ
Fig. 5　Bimorph type piezoelectric actuator.

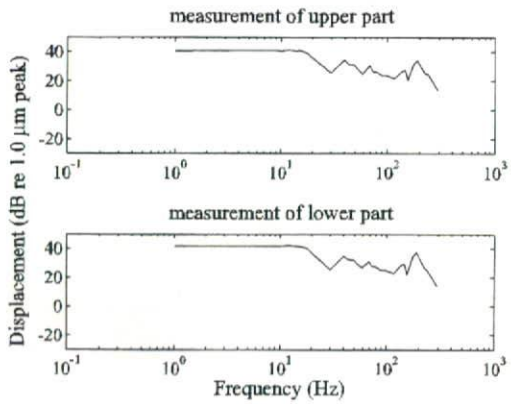

図 6　ピンの変位の比較（上部計測と下部計測）
Fig. 6　Comparison of pin displacement.

備してある．本研究では計測で印加電圧を明示することから，可変抵抗を廃し駆動周波数と駆動電圧を任意に設定できる制御回路を設計し製作した．

3.1.2　レーザ変位計

触知ピンの変位計測にレーザ式変位計（LE–4000）を用いた．このセンサは三角測量を応用した方式で，半導体レーザを用いた発光素子と CCD（Charged Coupled Device）受光素子によって構成されている．分解能は 0.1 μm であり，サンプリング周波数は 2 kHz である．また，最小スポット径は直径約 30 μm である．

3.2　被　験　者

被験者は 23 歳男性で，左手の示指を触知提示装置に置いて計測を行った．

4.　触知ピンの基本特性の計測

指の皮膚を変形させているのは指と接触している触知ピンの上面であり，本研究で実施する触知盤の下部からバイモルフ素子の変位を計測した場合との関係性を知る必要がある．上部から計測した触知ピンの上面の変位（以降，上部計測）と，下部から計測したバイモルフ素子の変位（以降，下部計測）とを計測し，両者の計測において同等の結果が得られることを示す．

4.1　実験条件

実験条件として，(1) 駆動電圧を 30 V とし，(2) 指と触知ピンが非接触，つまりピンは自由に振動できる状態を設定した．(3) 計測は次の各駆動周波数（1, 5, 9, 10, 12, 14, 15, 16, 18, 20, 30, 40, 45, 50, 60, 70, 75, 80, 90, 100, 120, 140, 150, 160, 180, 200, 230, 250, 300 Hz）で，(4) 触知ピンの挙動が定常になるまで十分な時間（約 5 s）をおいてから計測を開始した．(5) 解析は，各駆動周波数の 50 周期分のデータを取り出し，ドリフトを除去して変位のピークの平均値をプロットした．(6) なお，計測は 5 回行い再現性を確認した．

4.2　結果と考察

上部計測の結果を図 6 の上部に，下部計測の結果を図 6 の下部にそれぞれ示す．**5.** で比較を行うことからここでも縦軸は 1.0 μm ピークを基準にして，横軸の各振動周波数に対して dB 表示してある．

両者の相関係数は 0.996 であり差異は認められない．オプタコン–II の駆動周波数であり，後述の実験で用いる 230 Hz に注目すると，上部計測での変位は 22.0 dB となり，下部計測での変位は 22.2 dB となる．上部計測と下部計測との相対的な変位差が 0.2 dB 程度あるが，原因としてバイモルフ素子と触知ピンとの位置関係が常に直角でないことが考えられる（図 5）．

5.　指接触下での触知ピン変位計測（定常刺激）

本章では指と触知ピンとが接触している状況下での触知ピンの変位計測を行い機械的な特性を明らかにする．また，Bolanowski らの 4 チャネルモデルや Gescheider らが示した接触子形状のデータに当てはめ，オプタコン–II が刺激する機械受容ユニットの特定を行う．実験装置を図 7 に示す．

5.1　実験条件

実験条件として，(1) 刺激強度を変えるために触知ピンの駆動電圧を 10 V，30 V，50 V に設定し，(2)

指と触知ピンが接触，つまりピンは常に負荷を受けながら振動する状態を設定した．この際，ピンの刺激が知覚できる程度に触知盤に指を押し付けた．(3) 駆動周波数，(4) ピンの変位が定常状態に落ち着くまでの過渡期の影響の除去，(5) データの解析方法は **4.1** に準じる．(6) なお，計測は任意に選択した 5 本の触知ピンに対して行い，5 回繰り返し再現性を確認した．

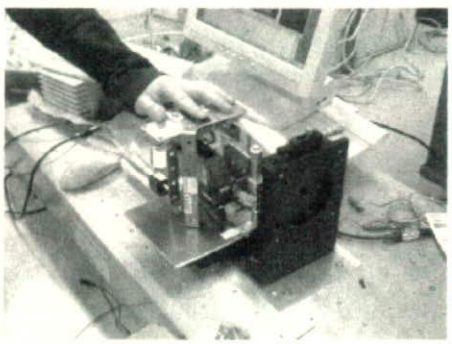

図 7 計測装置
Fig. 7 Measurement apparatus.

5.2 結果と考察

実験で得られた触知ピンの変位データを 1.0 μm ピークの振幅を基準に dB 表示したものと，四つの機械受容ユニットの振動検出しきい曲線との対比を，図 8〜図 11 に示す．前掲の Gescheider らによる振動検出しきい曲線も併せて記載する．

本研究の第一の目的であるオプタコン-II の機械特性の明示について，振動数対変位の関係に注目すると，実験を行ったすべての駆動電圧 10 V (△)，30 V (×)，50 V (+) において，振動数が高くなるにつれて変位は減少し，全周波数帯域での変位の底は駆動周波数 150 Hz となった．これらの結果は Bliss らの計

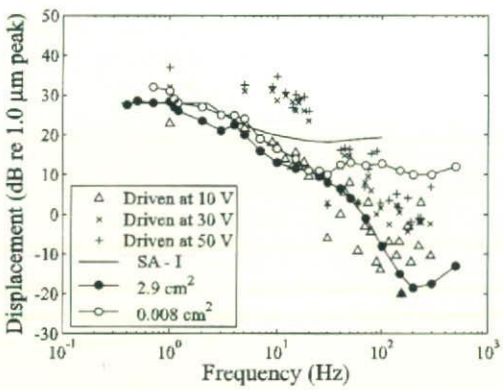

図 8 SA I と触知ピンの周波数応答
Fig. 8 Frequency response of SA-I and tactile pin.

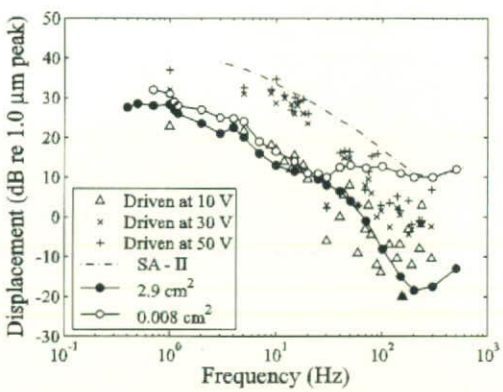

図 9 SA II と触知ピンの周波数応答
Fig. 9 Frequency response of SA-II and tactile pin.

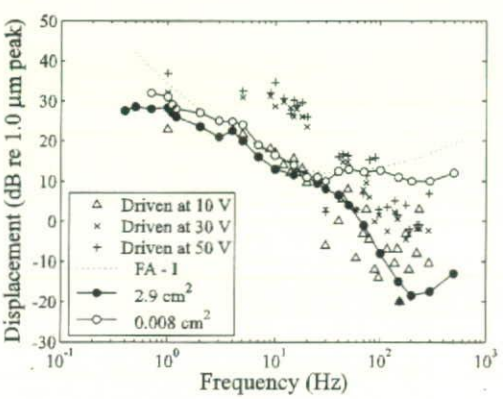

図 10 FA I と触知ピンの周波数応答
Fig. 10 Frequency response of FA-I and tactile pin.

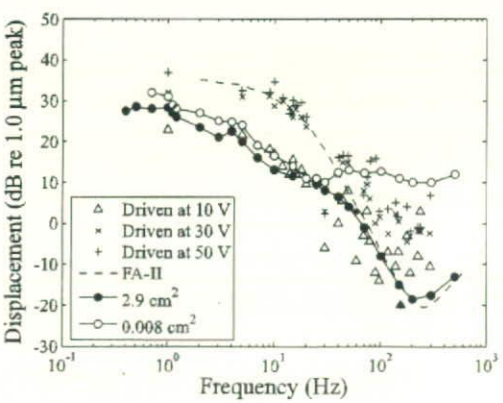

図 11 FA II と触知ピンの周波数応答
Fig. 11 Frequency response of FA-II and tactile pin.

測結果と異なる．駆動電圧対変位について，駆動電圧を 10 V，30 V，50 V と変化させたとき各駆動周波数での変位は比例関係になく，圧電アクチュエータは駆動電圧と変位が比例するとした既知の事実と異なる．原因としてピンは指との接触で応力を受けた状態で振動していることが考えられる．接触応力が変位に及ぼす影響は図 6 下部計測（非接触状態）の周波数特性と図 8～図 11（接触状態）の 30 V の周波数特性が異なることにも現れており，接触状態では非接触状態と比較して全周波数範囲で変位が減少し，高周波数帯で変位の減衰が顕著となる．減衰は皮膚の粘弾性特性の影響であると考えられる．

次に，各駆動周波数における触知ピンの変位と振動検出しきい曲線との対比から触知に関与する機械受容ユニットの特定を行う．仮に図 8～図 11 のような特性を備えたヒトを想定した場合，振動検出しきい曲線より下にある刺激は，対応する機械受容ユニットを介して感知されることはない．図 8 と図 10 から，SA–I と FA–I に対しては，駆動電圧が 30 V 以上であれば 20 Hz 以下の帯域でしきい値以上の振動刺激を与えられることが分かる．図 9 から，SA–II に対しては，全周波数帯域でしきい曲線以上の振動刺激は与えられない．図 11 によれば，FA–II に対しては，120 Hz 以上の駆動周波数であれば印加電圧に関係なく，ほぼ受容されるはずであるが，触知ピンの面積は 0.0007 cm^2（図 12）である．これは Gescheider らが例示する接触子面積 0.008 cm^2 より 1 けた小さいため，対応するしきい曲線は 0.008 cm^2 のそれより下がることはないと予想できる．いわゆる，FA–II 固有の空間的加重の効果であり，これを踏まえると 120 Hz 以上で 0.008 cm^2 のしきい曲線を超える変位はない．低及び中周波数帯域で，FA–II のしきい曲線近傍に変位がプロットされているが，それが平均値であること，その帯域では他の受容器が優勢であることを考慮すると，FA–II の関与は極めて低いと推測される．

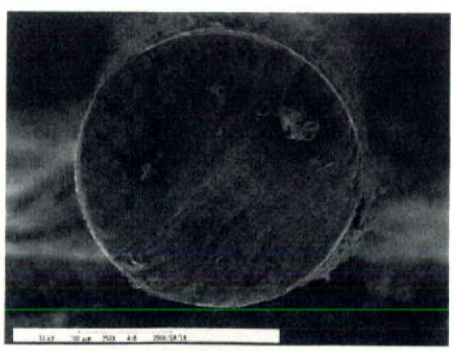

図 12　電子顕微鏡による触知ピン先端形状の撮像
Fig. 12　Picturization of the tip form of the tactile pin by an electron microscope.

6. 指接触下での触知ピン変位計測（間欠刺激）

オプタコン–II で文字を提示する場合，右利きのユーザは左手の示指を触知ピンアレーに乗せ，右手でスキャナを持つ．継続して文字をスキャンする過程で，任意の 1 ピンに注目すると，on と off とが不連続，かつランダムに生成されることになる．このとき指は振動・静止状態の間欠的な刺激を受けており，実際の使用条件ではほとんどがこの刺激であると考えられる．間欠刺激の例として，今，格子状に並べられた触知ピンアレーを 7 行 5 列に単純化してアルファベットの “A” を提示する触知ピンの挙動を考えてみる（図 13）．触覚提示装置の第 3 行 5 列目のピンの挙動に注目すると，このピンは “A” が図の (2)，及び (4) のように撮像されたときに振動する．本実験では触知ピンと指が接触した状況下において，振動・静止状態を間欠的に繰り返す触知ピンの変位を調べた．

6.1 実験条件

実験条件として，(1) 駆動電圧を 30 V とし，(2) 指と触知ピンは接触状態とした．この際，ピンの刺激が知覚できる程度に指を触知盤に押し付けた．(3) 駆動周波数は 230 Hz で，(4) 実験開始時からデータを収集し，(5) 掲載データのドリフトは除去した．(6) 計測回数は 5 回行い再現性を確認した．

6.2 結果と考察

図 14 に 0.4 s を 1 周期とした間欠刺激信号を送信したときのピンの変位を示す．初期状態から on 期間の開始とともに 33 μm（30 dB）の変位を生じ，その状態から 230 Hz で振動状態となった．ただしその変位は小さく約 0.8 μm（−2 dB）であった．また，off 期

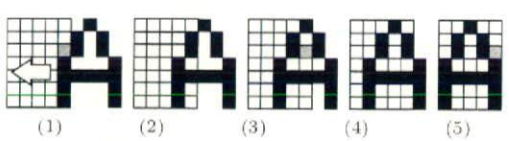

図 13　アルファベット “A” を提示する場合の各ピンの状態
Fig. 13　State of each pin showing alphabet “A”.

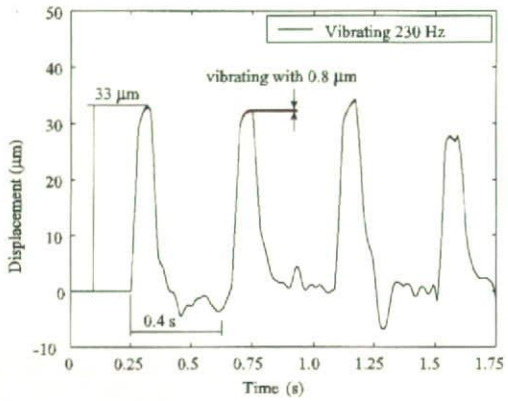

図 14 指接触下での触知ピンの変位計測（間欠刺激）
Fig. 14 Displacement measurement of the tactile pin in a finger contact state (intermittent stimulus).

間の開始とともに変位は初期位置に戻った．実験条件から，指は 0.4 s 周期で約 33 μm 変位させられる．単位を変換すると，2.5 Hz の振動数で約 30 dB の変位を受ける．これを図 1 に当てはめると，SA–I と FA–I だけが機能する周波数帯，及び変位となり SA–II や FA–II の関与は抑制されている．すなわち，オプタコン–II は空間分解能に優れる SA–I によって提示された形を知覚させることになり，このことは従来の触覚研究の知見とも合致するものである．

7. 総　　括

オプタコン–II は 230 Hz の高周波数で固定されて駆動されており，かつその変位も微小なものであるとの認識により，FA–II の振動検出チャネルを用いてユーザに情報を伝達すると漠然と考えられていた．しかしながら，オプタコン–II の触知ピンの接触子面積，変位，駆動周波数ではヒトの振動検出チャネルを刺激できないことが分かった．また，間欠刺激の実験から，オプタコン–II は間欠的に低周波数で出現する触覚的な情報に関して，形を SA–I に与え，低周波数で感度の高い FA–I で形の動きを与えていると考えられる．

実際のオプタコン–II での触読を想定すると，右手で持つスキャナを自らが動かすことにより触読のきっかけを自らが作っており，同時にその動かしている感覚を強調するように，FA–I が触知盤上の形の動きを検出し，提示パターンが変化していることを知覚する．提示パターンが動いているか否かを理解しながら，空間分解能に優れた SA–I で形認識を行い触読を容易にしていると考えられる．加えて，Johnson らが指摘しているように SA–I には形状認識に選択的な感受性が備わっており，エッジやカーブなどの形状認識では一定の背景上に浮彫り様の SA–I 神経イメージを作り出す．オプタコン–II の触知ピン変位調節機構は，こうした SA–I イメージの作成を容易にする．

スキャナの自由な移動速度とユーザに個別に異なる刺激強度の調節が容易に行えるシステム構成であることが，オプタコン–II で触読ができるメカニズムであり，当時視覚障害者の読書支援機器とされた理由であると考えられる．

8. む す び

本研究では，感覚代行器としての実績があり，心理物理実験での刺激提示装置として用いられるオプタコン–II の基本特性に注目して検討を行った．レーザ変位計を用いることで，微小である触知ピンの変位を計測し，ヒトの触覚特性との比較からオプタコンの基本特性の評価を行った．このとき，触知ピンが指に加える変位を計測するために，触知ピンの下部から変位を計測する実験装置を構築し，接触しているがゆえに変位している触知ピンの頂点が計測できないとした問題点を解消し，計測を可能とした．下部計測では上部計測と同等の計測が行えることを定量的に示し，指と触知ピンが接触している状況下での変位の計測データから 4 チャネルモデルと対応させ，オプタコン–II が刺激する機械受容ユニットの特定を行った．また，触知ピンの間欠的な挙動に注目し，計測・検討を行うことで，現在まで曖昧にされてきたオプタコン–II を用いて触読ができる根拠を与えた．本研究の知見は神経生理学の分野で触覚提示装置として広く用いられているオプタコン–II の機械的な基礎資料を与える．

文　　献

[1] D.T. Horner, "The effect of location on the discrimination of spatial vibrotactile patterns," Perception & Psychophysics, vol.57, no.4, pp.463–474, 1995.
[2] R.W. Cholewiak and A.A. Collins, "Individual differences in the vibrotactile perception of a simple pattern set," Perception & Psychophysics, vol.59, no.6, pp.850–866, 1997.
[3] L.J. Post and C.E. Chapman, "The effects of cross-modal manipulations of attention on the detection of vibrotactile stimuli in humans," Somatosensory & Motor Research, vol.8, no.2, pp.149–157, 1991.
[4] E.P. Gardner, C.I. Palmer, H.A. Hamalainen, and S. Warren, "Simulation of motion on the skin. 5. effect

of stimulus temporal frequency on the representation of moving bar patterns in primary somatosensory cortex of monkeys," J. Neurophysiology, vol.67, no.1, pp.37–63, 1992.

[5] E.P. Gardner and B.F. Sklar, "Discrimination of the direction of motion on the human hand — A phychophysical study of stimulation parameters," J. Neurophysiology, vol.71, no.6, pp.2414–2429, 1994.

[6] E.A. Lerner and J. Craig, "The prevalence of tactile motion aftereffects," Somatosensory & Motor Research, vol.19, no.1, pp.24–29, 2002.

[7] C.E. Kops and E.P. Gardner, "Discrimination of simulated texture patterns on the human hand," J. Neurophysiology, vol.76, no.2, pp.1145–1165, 1996.

[8] R.W. Cholewiak and A.A. Collins, "Vibrotactile pattern discrimination and communality at several body sites," Perception & Psychophysics, vol.57, no.5, pp.724–737, 1995.

[9] D.A. Gelber, M.A. Pfeifer, V.L. Broadstoner, E.W. Munster, M. Peterson, J.C. Arezzo, H. Shamoon, A. Zeidler, R. Clements, D.A. Greene, D. Porte, C. Laudadio, and V. Bril, "Components of variance for vibratory and thermal threshold testing in normal and diabetic subjects," J. Diabetes and its Complications, vol.9, no.3, pp.170–176, 1995.

[10] J.C. Stevens, "Aging and spatial acuity of touch," J. Gerontology, vol.47, no.1, pp.35–40, 1992.

[11] F.J. Winn and V. Putzanderson, "Vibration thresholds as a function of age and diagnosis of carpal-tunnel syndrome — A preliminary-report," Experimental Aging Research, vol.16, no.4, pp.221–224, 1990.

[12] J.C. Bliss, M.H. Katcher, C.H. Rogers, and R.P. Shepard, "Optical-to-tactile image conversion for the blind," IEEE Trans. Man-Machine Systems, vol.MMS-11, no.1, pp.58–65, 1970.

[13] J.C. Bliss, "A relatively high-resolution reading aid for the blind," IEEE Trans. Man-Machine Systems, vol.MMS-10, no.1, pp.1–8, 1969.

[14] S.J. Bolanowski, G.A. Gescheider, R.T. Verrillo, and C.M. Checkosky, "Four channels mediate the mechanical aspects of touch," J. Acoust. Soc. Am., vol.84, no.5, pp.1680–1694, 1980.

[15] G.A. Gescheider, S.J. Bolanowski, and K.R. Hardick, "The frequency selectivity of information-processing channels in the tactile sensory system," Somatosensory & Motor Research, vol.18, no.3, pp.191–201, 2001.

[16] R.S. Johansson and A.B. Vallbo, "Tactile sensory coding in the glabrous skin of the human hand," Trends in Neurosciences, vol.6, pp.27–32, 1983.

[17] F. Vega-Bermudez and K.O. Johnson, "Surround suppression in the responses of primate sa-i and ra mechanoreceptive afferents mapped with a probe array," The American Physiological Society, pp.2711–2719, 1999.

[18] J.G. Linvil and J.C. Bliss, "A direct translation reading aid for the blind," Proc. IEEE, vol.54, no.1, pp.40–51, 1969.

付　　録

ここでは，**6.** の実験で用いた実験条件の妥当性を示す．**6.** では実験条件として間欠刺激を 0.4 s 周期とした．今，オプタコン-II の触知ピンが間欠刺激 0.4 s 周期で形状呈示しており，ユーザが 1 回の形状呈示で形を認識できるとすれば毎秒 2.5 文字，つまり毎分 150 文字触読できる．Bliss の定義に従い 1 単語をアルファベット平均 5 文字とすれば毎分 30 単語触読できることになる．更に Bliss の実験結果を引用すると被験者 3 名のうち 1 名が 17 時間，2 名が 50 時間のトレーニングの後，毎分 30 単語触読可能であったと報告されている．オプタコン II を用いた触読で毎分 30 単語触読する状況は存在しており，本実験で設定した間欠刺激条件は妥当であると考える．

（平成 18 年 11 月 22 日受付，19 年 8 月 15 日再受付）

島田　茂伸

平 16 北海道大学大学院工学研究科博士後期課程了．同年電気通信大学 SVBL 非常勤研究員．平 18 東京都立産業技術研究センター研究員．電気通信大学特別研究員併任．以来，ロボティクス・メカトロニクスの研究，特に触覚を用いたインタフェース方式の研究開発に従事．日本 VR 学会学術奨励賞（平 18）受賞．日本機械学会，日本ロボット学会，計測自動制御学会，日本バーチャルリアリティ学会等各会員．博士（工学）．

篠原　正美

昭 45 東工大・理工・数学了．同年通産省工業技術院製品科学研究所入所．機構改革に伴い，生命工学工業技術研究所，産業技術総合研究所に勤務し，平 19 退職．この間，仏マルセイユ大学医学部客員研究員，人間工学，認知科学，福祉工学の研究に従事．現在は，産業技術総合研究所能力開発部門で，障害者就労環境の整備に関与している．IEEE，日本数学会会員．

安彦　成泰

平 16 電気通信大学大学院機械制御工学研究科修士課程了．同年帝人ファーマ株式会社入社．以来，在宅医療に用いる酸素濃縮器の研究開発に従事．

下条　誠　（正員）

昭 51 東京工業大学大学院総合理工学研究科精密機械システム専攻了．同年通産省工業技術院製品科学研究所入所，平 9 茨城大学工学部情報工学科教授，平 13 電気通信大学電気通信学部知能機械工学科教授，現在に至る．この間，昭 60 年 9 月から 1 年間米国スタンフォード大学工学部客員研究員．ロボティクス・メカトロニクスの研究に従事．触覚センシング，ロボットハンド，触覚を用いたインターフェース方式の研究開発を行っている．日本機械学会，日本ロボット学会，日本バーチャルリアリティー学会各会員．日本機械学会フェロー．博士（工学）．

2008 IEEE/RSJ International Conference on Intelligent Robots and Systems
Acropolis Convention Center
Nice, France, Sept, 22-26, 2008

Development of High Speed and High Sensitivity Slip Sensor

Seiichi Teshigawara*, Masatoshi Ishikawa**, Makoto Shimojo*

Abstract— **Slip detecting tactile sensors is essential to achieving a human-like gripping motion with a robot hand. Up until now, we have developed flexible, thin and lightweight center of pressure (CoP) sensor. The sensor, constructed of pressure conductive rubber sandwiched between two sheets of conductive film, is able to detect the center position of the load distribution and the total load. Recently, detection of initial slip has been shown to be possible. However the detection principles are unclear. Therefore, we carried out verification experiments of the slip detection properties of the CoP sensor and the detection principle. In the results, we found a change in electrical conductivity produced with a shear deformation of the pressure conductive rubber. In this paper, we will discuss the slip detection properties of the CoP sensor and detection principle.**

I. INTRODUCTION

With the aim of achieving a human-like robot hand, or one that is superior to the human hand, much research has been carried out [1][2][3]. Even with eyes closed, humans can grip with minimum force an object with unknowns such as weight and coefficient of friction, etc. We are also able to perform smoothly such motions as handing the object off or setting it down. To achieve these motions with a robot hand requires tactile sensors having slip sense in addition to contact position and load.

Johansson et al. [4][5], in their research regarding the gripping motion of humans, made clear that humans grip objects at the minimum gripping force that is close to producing slip. It was also shown that the initial slip between the skin and the gripping object was essential to this sense. Therefore, up until now various slip sensors detecting initial slip have been proposed. Trembley et al. [6] developed a sensor, arranging acceleration sensors in sets of two inside a spherical silicon rubber with a projection called a "nib", that detected the vibrations which occur on the surface of the sensor as a result of initial slip. Son et al. [7] developed a sensor with four sheets of PVDF film arranged in a semi-circular silicon rubber tube that similarly detected the vibrations occurring from initial slip. Adding to the findings of Johansson et al., Maeno et al. [8] modelled the structure of the finger pad by means of finite element analysis and made clear the properties of individual tactile receptors. They then imitated the human gripping technique, developing sensors lined up inside a curved elastic surface at regular intervals along a strain gauge [9]. With this, they showed that it was possible to grip an object of unknown weight and coefficient of friction. Shinoda et al. [11] proposed a slip sensor using Acoustic Resonant Tensor Cell (ARTC). The ARTC is composed of a resonance cavity within the elastic body and ultrasonic receiving probe; the slip direction stress is detected from changes in the ultrasonic wave resonance frequency. Ikeda et al. [12] observed the contact surface between an elastic body and a rigid plate by utilizing a camera, and proposed a technique for estimating slip margin.

As shown above, much research has been conducted regarding slip sensors. However, as yet, a practical slip sensor does not exist. This is thought to be for the following causes. Firstly, there is the problem of reduction in size and weight. The space where sensors can be located for most robot hands is limited from the point of view of mechanism function. Accordingly, structures with devices embedded inside the fingers and thick sensors are undesirable. Secondly, there is the problem of wiring. When sensors using strain gauges or PVDF films are configured over a large area, it is necessary to increase the number of sensing elements and wires. However, excessive wiring becomes a burden on the hand. Finally, there is the problem of response. Especially when cameras are used, response is dependent on the processing time of the data. Since a delay in response time increases the slip displacement of the object, high-speed response is desirable.

Therefore, in this research, our goal is to develop thin, lightweight slip sensors with high-speed response that could be installed on existing robot hands. Until now, we have carried out the research and development of "The Center of Pressure (CoP) tactile sensor" for detecting two-dimensional load distribution with the following properties [13].

1) Flexible, thin(approximately 0.7 mm), lightweight(approximately 0.2 g/cm^2)
2) Wire saving(4$wires$)
3) High speed responsibility(1ms)

The CoP sensor can detect the center of the load distribution and the total load added to a surface. In recent experiments, it was found that these could be utilized as sensor to detect the initial slip as well [14]. By using this sensor, we succeeded in holding the glass whose weight changes (as shown in Fig.1). However, the detailed detection mechanism is unclear. In this paper, we will simply mention the slip detection experiment using the CoP sensor, and report on the slip detection properties and mechanism.

II. CoP TACTILE SENSOR

A. Pressure Sensitive Conductive Rubber

Pressure conductive rubber (product of Inaba Rubber Co., Ltd.) has the function of converting pressure into electrical

*Mechanical Engineering and Intelligent Systems, The University of Electro-Communications, 1-5-1 Chofugaoka, Chofu-shi, 182-8585 JAPAN
**Department of Information Physics and Computing, Graduate School of Information Science and Technology, The University of Tokyo, 7-3-1 Hongo, Bunkyo-ku, Tokyo 113-0033, Japan

978-1-4244-2058-2/08/$25.00 ©2008 IEEE.

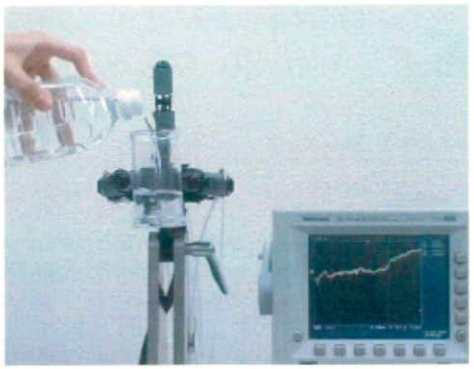

Fig. 1. Grasping force control for the object whose weight change (pouring water into a cup)

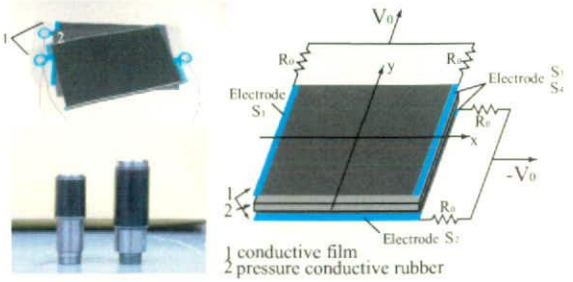

Fig. 2. Structure of the CoP sensor

resistance. It is a high polymer material primarily composed of silicon rubber, and conductive carbon particles are uniformly distributed. An increase in the pressure causes a decrease in volume, and the carbon particles contact each other forming conduction routes. In other words, due to the deformation of the rubber caused by increasing pressure, there is a change in the distribution of carbon particles inside the rubber. The fluctuation in the number of conduction routes due to the carbon contacts appears as a change in electrical resistance.

B. Structure, Theory, and Properties

As shown in Fig. 2, the structure of the CoP sensor is that pressure conductive rubber sandwiched between upper and lower layers of conductive film. At the edges of both layers of conductive film are electrodes (S_1, S_2, S_3, S_4). The center position of the load distribution is measured by the center position of the current distribution obtained from the potential difference across the electrodes (S_1-S_3,S_2-S_4). The load output is measured by the total electric current flowing to upper and lower layers. Structurally, the CoP sensor is flexible, thin, and lightweight, and may be arranged on a cylindrical surface (Fig. 2, lower-left). The number of wires is four, which is not dependent on the area of the sensor. Moreover, the filter circuit is not used because this sensor is strong in the high frequency noise in practical level like force-feedback control. This sensor has a high-speed response of less than 1 (ms) because the circuit is only an analogue arithmetic circuit. Therefore, this sensor is suitable for the control system of a robot hands.

III. Slip Detection Experiment with The CoP Sensor

In this experiment, we show that the CoP sensor can detect the initial slip. So, we compared the CoP sensor load output with the gripping force measured by a load cell. The experimental apparatus utilized in this experiment is shown in Fig. 3. The CoP sensors were arranged around two cylinders (diameter 18 mm), and fixed face-to-face using a special purpose jig. The height and tilt of the CoP sensors were regulated by a left θ-stage and a right XYZ-stage. As in the figure, the plastic cylinder (18 mm) was sandwiched by the CoP sensors (Fig. 3-(1)), and this was connected by wire to the tension side load cell (we call "Load cell(Z)" below). Load cell(X) in Fig. 3 denotes the normal vector force (gripping force) and Load cell(Z) denotes the tangential force (tensile force). The gripping force was adjusted to 2 N while seeing Load cell (X) output. When the automatic Z-stage was activated, the gripping object was made to slip downward vertically (Fig. 3-(2)). Since it was possible to regulate the speed of the automatic Z-stage from 1 $\mu m/s$ to 100 mm/s, we can control the slip velocity of the plastic cylinder. The velocity for this experiment was set at 100 mm/s. The slip displacement of the plastic cylinder was measured by a laser displacement sensor (resolution: 0.1mm).

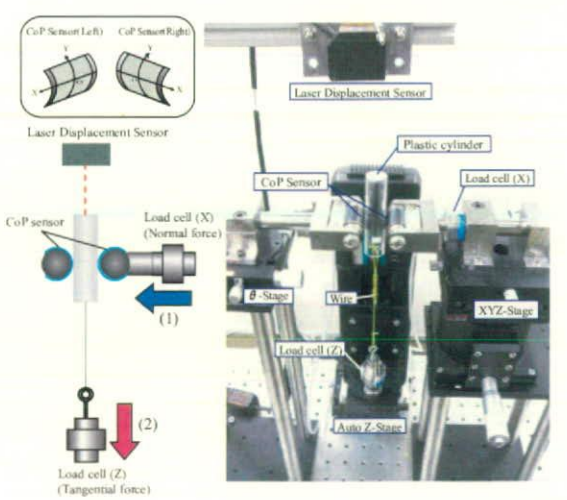

Fig. 3. Experimental apparatus for slip detection using the CoP sensor

A. Experimental Results

The results of this experiment are shown in Fig. 4. The graphs show, from top to bottom, (a) the CoP sensor load output, (b) the CoP sensor position output, and (c) two load cells and laser displacement sensor output. As the left and

right CoP sensor position output was the same, only the right side position output of the CoP sensor is shown. From the laser displacement sensor output, the slip displacement occurs from the time of the vertical line shown on the graph.

We compared the CoP sensor load output with the grip force according to Load cell (X). Looking at the grip force, its change was approximately 0.2 N and increasing just before the occurrence of slip displacement. Slip displacement occurs when a initial slip changed to a global slip. At this point, we can consider the gripping object and sensor surface to be detached for an instant, and that the load in the normal vector direction increased. Meanwhile, looking at the CoP sensor load output, there is a large decrease just before the occurrence of the slip displacement. The right side CoP sensor output decreased by approximately 4 V. According to the sensor load output characteristics, a decrease of approximately 1 N was produced. There was a decrease of approximately 1.3 N at the left side CoP sensor. We can say that the change is not one-sided because there was a simultaneous decrease in left and right outputs. In spite of the increase in the grip force, the CoP sensor's load output of both sides decrease before slip displacement occurs. So, using these changes, it is possible to detect the start of slip (referred to as "initial slip").

Meanwhile, the change in the CoP sensor's position output (Fig. 4-(b)) was extremely small, only about 0.05 V circumferentially against $\pm 4V$ full scale. This may be considered the change between stick area and slip area produced when the gripping object slips along the sensor surface [10]. This small change was due to the small contact area as a result of cylinder-to-cylinder contact. So, we install a silicon rubber on the CoP sensor surface, and increasing the contact area. Consequently, we were able to increase the change of the CoP sensor's position output two or four times. It is possible to detect the slip direction using the position output change because this change is only produced in the slip direction (circumferential direction in this case).

B. Discussion

The above results show that the CoP sensor can detect the initial slip and the slip direction. We expect that the change of the CoP sensor's load output (Which we call "slip output" below) is produced by the following phenomena. Looking at the colored area of Fig. 4-(a) and (c), the CoP sensor's load output begins to decrease at the same instant, and we find that the tangential force (Load cell(Z) output) also begins to increase. From this, we can expect that a shear deformation of pressure conductive rubber occur by the tangential force. On the other hand, the change of the CoP sensor's load output is dependent on the electrical resistance change of the pressure conductive rubber. This indicates that there is some relationship between the shear deformation of the pressure conductive rubber and the change of electrical resistance. So, we conducted an experiment to observe the change of electrical resistance when pressure conductive rubber undergoes a shear deformation.

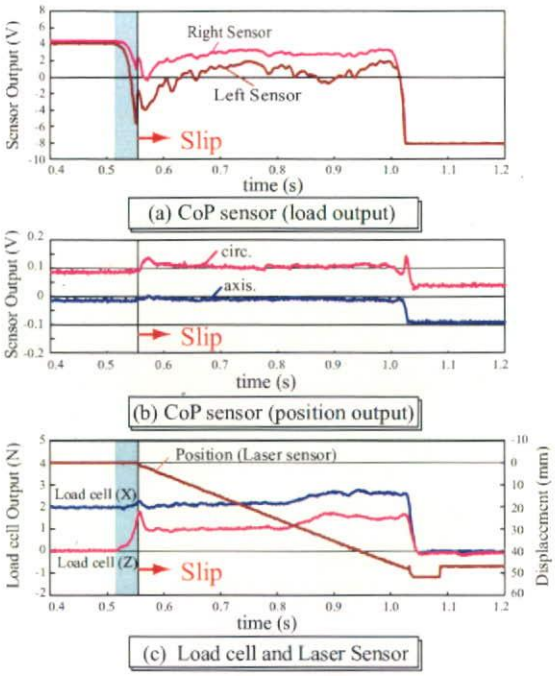

Fig. 4. Result of Slip detection experiment

IV. Pressure Sensitive Conductive Rubber Shear Deformation Experiment

A. Experimental Method

In this experiment, we reveal why CoP sensor's output change when an object slips on the CoP sensor. So, we inserted pressure conductive rubber electrodes, and measured the voltage between electrodes when it was made to undergo a shear deformation. The experimental apparatus is shown in Fig. 5. The electrodes (gold plated) were attached to acrylic plates, which were aligned facing each other (the circled area of Fig. 5). In the experiment, the electrodes were connected to a regulated power supply through a resistance of 1 $k\Omega$, and a voltage of 5 V was applied.

The X-stage installed on the right side of the experimental apparatus was activated, and the pressure conductive rubber (7 mm^2) was sandwiched between the electrodes (Fig. 5-(1)). This X-stage was equipped with a dedicated actuator, with a travel speed of 0.1 mm/s and a positioning accuracy of 0.017 mm. Therefore, the quantity of the normal direction deformation of the pressure conductive rubber could be finely controlled. The X-stage was activated again, and the normal direction load was increased. At this time, the voltage between electrodes was decreased from 5 V (load cell output : 0N) to 2 V (load cell output : approximately 1.7 N). From now on, this voltage is referred to as initial voltage (V_i).

Next, the automatic stage installed on the left side was activated producing a shear deformation of pressure conductive rubber (Fig. 5-(2)). The automatic stage had a positioning

accuracy of 0.012 *mm* and its speed could be adjusted from 1 $\mu m/s$ to 100 mm/s. The quantity of the shear deformation of the pressure conductive rubber could be measured by the laser displacement sensor (resolution 0.1 μm). In this experiment, the shear deformation of the pressure conductive rubber was set to 0.3 *mm*, and the three deformation speeds was set such as 0.05 mm/s, 0.1 mm/s, and 1 mm/s. The voltage between electrodes and the laser displacement sensor output were measured.

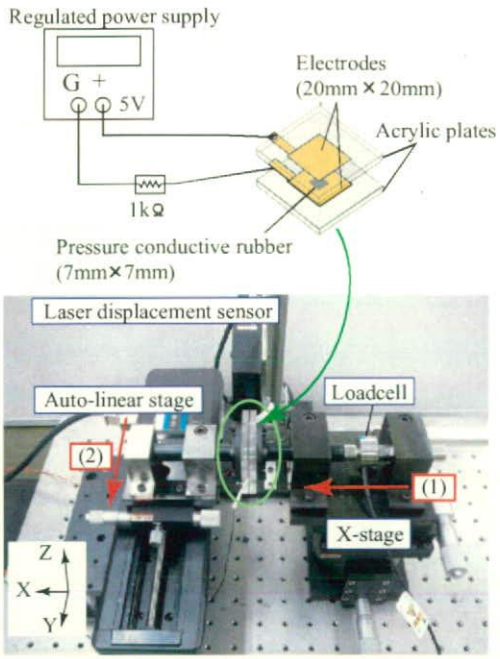

Fig. 5. Experimental system for deformation of pressure conductive rubber

B. Experimental Results

The results of the experiment are shown in Fig. 6, Fig. 7 and Fig. 8. Time (s) is along the horizontal axis and the voltage between electrodes and laser displacement sensor output (*mm*) are along the vertical axis. At all deformation speed, the voltage increased, when the shear deformation of the pressure conductive rubber was occurred by the Auto-linear stage. Taking the rise of the voltage at this point as ΔV, a summary of the voltage difference ΔV is shown in Table I. Moreover, the voltage remained constant during shear deformation of the rubber. When the shear deformation stopped, the voltage gradually decreased and converge to about 3 *V*.

TABLE I

CHANGE OF VOLTAGE BETWEEN ELECTRODES

Shear deformation speed(mm/s)	$\Delta V(V)$
0.05	1.4
0.1	1.6
1	2.1

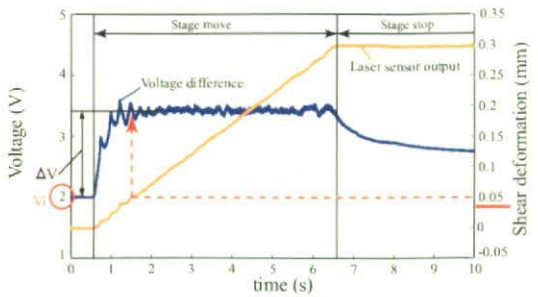

Fig. 6. The voltage difference between electrodes, shear deformation speed : 0.05mm/s

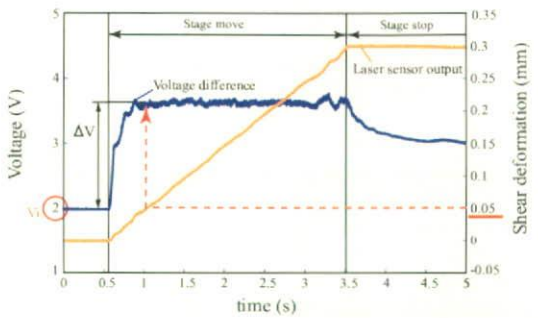

Fig. 7. The voltage difference between electrodes, shear deformation speed : 0.1mm/s

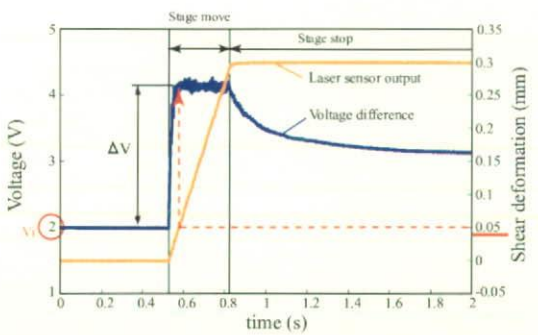

Fig. 8. The voltage difference between electrodes, shear deformation speed : 1mm/s

C. Discussion

1) Change in Electrical Resistance of Rubber: There was a large rise in the voltage between electrodes at the time of the shear deformation of the pressure conductive rubber. The rise of voltage indicated an increase in the electrical resistance of the rubber. As in the above hypothesis, we found that a change of electrical resistance was produced when a shear deformation of the rubber occurred. This fact was designated as a decrease in the load output of the CoP sensor. Looking at the results of the 0.05 mm/s trial, the voltage difference ΔV raised more than 1 *V* with a shear deformation of only 0.05 *mm*. This time, there was a large increase in the electrical resistance of the pressure conductive rubber. This was the same in the 0.1 mm/s and 1 mm/s trials. This agrees with the large decrease of the CoP sensor load output that occurred before the change

in the laser displacement sensor output utilized in section III. Therefore, it is clear that the slip output of the CoP sensor was generated by the change in electrical resistance of the pressure conductive rubber at the time of its shear deformation.

The rise in the electrical resistance of the pressure conductive rubber can be considered to be due to the following reasons. The pressure conductive rubber was a high polymer material primarily composed of silicon rubber with carbon particles uniformly distributed within. In an unloaded condition, the carbon particles were separated from each other as in Fig. 9-(a), so even if a voltage was applied, electric current would not flow. However, when the pressure was increased, the distribution of the carbon particles inside the rubber changed, and the carbon particles contacted each other as in Fig. 9-(b) forming a conduction route. As mentioned in section II-A, when there is an increase in conduction routes due to contact of carbon particles in pressure conductive rubber, this appears as a change in electrical resistance. Therefore, if we add a shear deformation to pressure conductive rubber as in Fig. 9-(c), the conduction routes fragment, and the number of conduction routes decreases. This situation shows the electrical resistance to increase. When the deformation stops, as in Fig. 9-(d), the conduction routes inside the rubber are restored. So, the electrical resistance seems to gradually decrease. In this experiment, the voltage converge to about $3V$ (as shown in Fig.6, Fig.7, Fig.8). But the voltage differences don't reach the same final value completely and it takes about 5 seconds to reach the stable value. The cause is regarded as an influence of hysteretic of pressure conductive rubber.

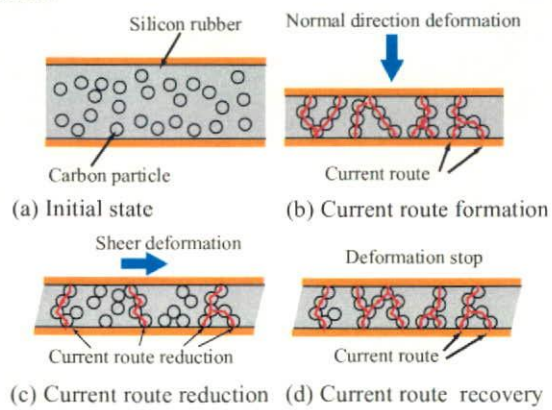

Fig. 9. Structure of Pressure conductive rubber

2) Speed of Rubber Shear Deformation: Here we shall discuss the relationship between the shear deformation speed of the pressure conductive rubber and the change of voltage between the electrodes. As shown in Table I, the size of the voltage difference ΔV changes according to the deformation speed of the rubber. This change tends to be significant as the deformation speed becomes greater. Accordingly, the shear deformation speed was varied at appropriate intervals from 10 $\mu m/s$ to 4000 $\mu m/s$, and the new voltage differences were measured. The voltage differences ΔV for each shear deformation speed plotted in a double-logarithmic graph are shown in Fig. 10. The voltage differences ΔV for initial voltages (initial loads) measured at 3 V (load cell output: approximately 1.0 N) and 4 V (load cell output: approximately 0.5 N) were shown in the same graph. This graph showed a linear increase in voltage difference ΔV accompanying increases in the shear deformation speed (v_s) of the rubber. Regarding the conductive mechanism of pressure conductive rubber, the following items are to be considered. With slow shear deformation, only deviation in the conduction routes are produced and they are not fragmented. Meanwhile, with rapid deformation, conduction routes that were not fragmented with slow deformation are broken due to the sudden deformation. Therefore, the voltage difference ΔV increased more with rapid shear deformation.

Consequently, when we measure the initial voltage (V_i) and the voltage difference (ΔV), we find the shear deformation speed (v_s) of the rubber. The numerical formula in Fig. 10 conducts power approximation for each of these results with regression equations. Table II shows a constant (k) and an exponent (n) of the shear deformation speed (v_s). The line joining the three is can be represented the following formula:

$$\Delta V = k \times v_s^{0.11} \tag{1}$$

Fig.11 shows a graph with the initial voltage (V_i) from Table II along the horizontal axis and the constant (k) on the vertical axis. This graph is linear, so we find that the initial voltage (V_i) and the constant (k) are proportional. The relational expression for these is shown below.

$$k = -0.27V_i + 1.55 \tag{2}$$

From above, the shear deformation speed (v_s) of the rubber can be expressed with the following formula.

$$v_s = \left(\frac{\Delta V}{-0.27V_i + 1.55}\right)^{-0.11} \tag{3}$$

This formula shows that if we measure the initial voltage (V_i) when pressure conductive rubber is deformed in the normal vector direction and the change of voltage between electrodes (ΔV) when it is made to undergo a shear deformation, we can detect the speed of the shear deformation of the rubber.

TABLE II
CONSTANT AND EXPONENT OF FORMULA IN FIG. 10

Initial voltage (V_i)	Constant (k)	Exponent (n)
2	0.99	0.12
3	0.75	0.11
4	0.45	0.11

V. SUMMARY

To investigate the slip detection properties of the CoP sensor, an experiment comparing the outputs of a load cell and the CoP sensor was conducted. The results showed that the CoP sensor's load output varied with slip of the object being gripped. This change was more sensitive than a laser displacement sensor (resolution 0.1 mm), and so it

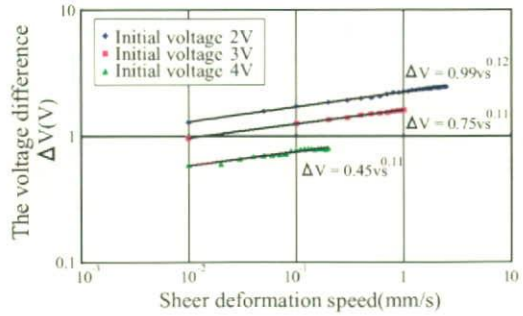

Fig. 10. Relation between the voltage difference of electrodes and shear deformation speed

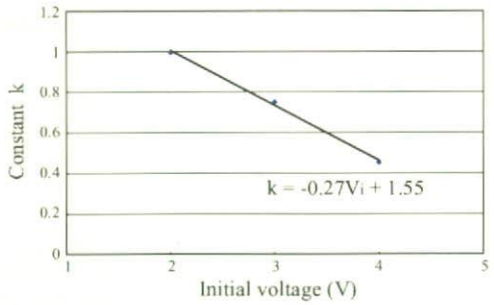

Fig. 11. Relation between constant k and initial voltage V_i

could be utilized to detect the initial slip. An experiment in which pressure conductive rubber was made to undergo a shear deformation was also conducted to clarify the CoP sensor slip detection mechanism. We found that when the pressure conductive rubber underwent a shear deformation, the resistance greatly increased. It was made clear that the load output change of the CoP sensor depends on the special properties of pressure conductive rubber when an object slipped over the sensor.

It is suggested that, through this experiment, the slip sensor without the CoP sensor could be configured using pressure conductive rubber. For example, when the simplest structure of pressure conductive rubber sandwiched between two electrodes is used, as in this experiment, the object is set on the sensor, made to slip, and simultaneous with it slipping, the voltage between electrodes changes. By measuring this change, it is possible to detect slip very clearly. When pressure conductive rubber is utilized to configure a slip sensor, considering the special properties, it will have the following characteristics.

Since the pressure conductive rubber is thin, approximately 0.5 *mm*, and light, so even with the electrodes are attached, a thin, lightweight sensor can be configured. As there is a change in the voltage between electrodes with a shear deformation of only 0.05 *mm* as shown in the shear deformation experiment, it is extremely high sensitivity. The sensor has a high-speed responsibility. As shown in section IV-C.2, if the shear deformation speed of the rubber (V_s) and the speed of slip of the object are set equal, the slip speed of the object can be detected from the voltage difference (ΔV) at the time of the shear deformation and the initial voltage (V_i), as in formula (3).

Up until now, there have been many slip sensors utilizing PVDF, strain gauges, cameras, etc. These sensors are difficult to detect initial slip without special structures, signal conditioning and filtering. However, our sensor using pressure conductive rubber can detect initial slip easily and clearly. So, we will conduct more detailed experimental analysis regarding the properties of pressure conductive rubber, and apply it to slip sensors.

REFERENCES

[1] Noriatsu Furukawa, Akio Namiki, Taku Senoo and Masatoshi Ishikawa, *Dynamic Regrasping Using a High-speed Multifingered Hand and a High-speed Vision System*, Proc. IEEE Int. Conf. on Robotics and Automation, pp.181-187, 2006

[2] H. Kawasaki, T. Komatsu, K. Uchiyama, *Dexterous Anthropomorphic Robot Hand With Distributed Tactile Sensor : Gifu Hand II*, IEEE/ASME Trans. Mechatronics, Vol7, No.3, pp.296-303, 2002

[3] L. Zollo, S. Roccella, E. Guglielmelli, M.C. Carrozza, P. Dario, *Biomechatronic Design and Control of an Anthropomorphic Artificial Hand for Prosthetic and Robotic Applications*, IEEE/ASME Trans. Mechatronics, Vol12, No.4, pp.418-429, 2007

[4] R.S. Johanson, G. Westling, *Roles of glabrous skin receptors and sensorimotor memory in automatic control of precision grip when lifting rougher or more slippery objects*, Exp Brain Res, Vol.56, pp. 550-564, 1984

[5] R.S. Johanson, G. Westling, *Signals in tactile afferents from the fingers eliciting adaptive motor responses during precision grip*, Exp Brain Res, Vol.66, pp. 141-154, 1987

[6] M.R. Trembly, M.R. Cutkosky, *Estimating Friction using Incipient Slip Sensing During a Manipuration Task* , Proc. IEEE Int. Conf. on Robotics and Automation, pp.429-434, 1993

[7] J.S. Son, E.A. Monteverde and R.D. Howe, *A Tactile Sensor for Localizing Transient Events in Manipulation*, Proc. IEEE Int. Conf. on Robotics and Automation, pp.471-476, 1994

[8] T. Maeno, K. Kobayashi, N. Yamazaki, *Relationship between Structure of Finger Tissue and Location of Tactile Receptors*, JSME Trans, Series C, Vol.63, No.607, pp.881-888, 1997(in Japanese)

[9] Y. Koda, T. Maeno, *Grasping Force Control in Master-Slave System with Partial Slip sensor*, Proc. IEEE/RSJ Int. Con. on Intelligent Robots and Systems, pp.4641-4646, 2004

[10] T. Maeno, S. Hiromitu, T. Kawai, *Control of Grasping Force by Detecting Stick/slip Distribution at the Curved Surface of an Elastic Finger*, Proc. IEEE Int. conf. on Robotics and Automation, pp.3895-3900, 2000

[11] H. Shinoda, S. Sasaki, K. Nakamura, *Instantaneous Evaluation of Friction based on ARTC Tactile Sensor*, Proc. IEEE Int. Conf. on Robotics and Automation, Vol.3, pp.2173-2178, 2000

[12] A. Ikeda, Y. Kurita, J. Ueda, Y. Matsumoto, T. Ogasawara, *Grip force control for an elastic finger using vision-based incipient slip feedback*, IEEE/RSJ Int. Con. on Intelligent Robots and Systems, pp.810-815, 2004

[13] M. Ishikawa, M. Shimojo, *A Method for Measuring the Center Position of a Two Dimensional Distributed Load Using Pressure-Conductive Rubber*, SICE Trans. vol.18, no.7, pp.730-735, 1982 (in Japanese)

[14] D. Gunji, Y. Mizoguchi, S. Teshigawara, A. Ming, A. Namiki, M. Ishikawa, M. Shimojo, *Grasping Force Control of Multi-fingered Robot Hand Based on Slip Detection Using Tactile Sensor*, Proc. IEEE Int. conf. on Robotics and Automation, pp.2605-2610, 2008

SICE Annual Conference 2008
August 20-22, 2008, The University Electro-Communications, Japan

A Net-Structure Tactile Sensor Covering Freeform Surface with Reduced Wiring

Makoto Shimojo[1] Takuma Araki[1] Masahiro Teranishi[1] Aigou Ming[1] Masatoshi Ishikawa[2]
1: Mechanical Engineering and Intelligent Systems,The University of Electro-Communications,
1–5–1 Chofugaoka, Chofu-shi, 182-8585 JAPAN, shimojo@mce.uec.ac.jp
2: Department of Information Physics and Computing,Graduate School of Information Science
and Technology, The University of Tokyo,7–3–1 Hongo, Bunkyo-ku, Tokyo 113-0033, Japan

***Abstract*— A tactile sensor is developed with the aim of covering a robot's entire structure, while reducing wiring requirement and ensuring high-speed response. There are only 4 signal wires from the sensor. The sensor response time is nearly constant (within 1ms) regardless of the number of detection elements, their placements or sensor areas. In this paper, the principles behind the operation of this sensor and the results of experiments using the sensor are described.**

I. INTRODUCTION

In recent years, research efforts to develop robots with tactile perception in order to achieve better safety in humans/robot shared environments and to enable effective communication with humans have been progressing[1]-[12]. However, many of these researches encountered some problems requiring resolution, such as those described below.

1) Covering free-form surfaces: Most robot bodies have freeform surfaces, making it hard to attach sensors.
2) Excessive wiring: A lot of wires are required in attaching multiple detection elements to a robot.

In this study, a net-structure tactile sensor attachable to freeform surfaces and with reduced wiring requirement was developed. The sensor features high response speeds without requiring software processing, is formed into a structure resembling a net, can be attached to freeform surfaces, and can detect the center of the load distribution as well as the overall load on 2-dimensional surfaces.

Fig.1 shows the conceptual schematic diagram of the sensor. There are only 4 signals from the sensor and Internal connection is required only between adjacent detection elements. Since the structure is like that of a net, the system of sensors can cover 3-dimensional freeform surfaces. Sensor response speed is almost unaffected by the number, placement, or sensor surface area of the detection elements. In summary, the sensor features the following:

1) Covering freeform surfaces: the sensor can be laid out like a net to cover freeform surfaces
2) Reduced wiring:Lines from the sensor consist of 4 wires only regardless of number, surface area, or placement of detection elements
3) High-speed response: response time is less than 1 ms regardless of number of detection elements. This means that the sensor is adequate for use in control loops around 1khz, which is the standard used in robotics control

II. SENSOR STRUCTURE

Sensor structure is shown in Fig. 2. The sensor is composed of tactile elements laid out on a matrix format. Each tactile element has one pressure-sensitive material r_p and four resistors r, as shown in the figure. The electrical resistance of the pressure-sensitive material decreases when load is applied to it. The sensor connects the tactile elements in an $m \times n$ matrix, and the electrical boundary conditions are imposed at the edge of the resistance network for an upper (layer A) and a lower (layer B), as shown in the figure. Sensor output is the voltage coming from the 4 electrodes E_1,E_2,E_3 and E_4.

III. PRINCIPLE OF THE SENSOR

The principle governing the sensor is the same as that for the sensor which we have developed and reported previously[14][15]. In this study, we extended the principle of the previous sensor to apply on discrete analog-network structures. When distributed load is applied to the sensor, the resistance r_p of the tactile element will change accordingly and the current $I(i,j)$ which flowing through resistance r_p will change. Thus, the current distribution in the sensor follows the load distribution. The sensor detects the center position of the current distribution as well as the total current flowing through.

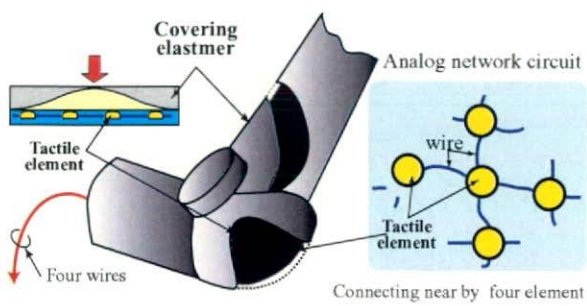

Fig. 1. Conceptual diagram of net structure tactile sensor

PR0001/08/0000-0904 ¥400 © 2008 SICE

A. Equivalent circuit and basic equation

The equivalent circuit near the tactile element(i, j) is shown in Fig.3. The current flowing from layer A into layer B through r_p is set to $I(i, j)$. The voltage $V_a(i, j)$ and $V_b(i, j)$ is impressed on the layer A and B respectively. Let us consider layer A. Referring to the equivalent circuit, Eq. (1) is derived from Kirchhoff's current laws as follows;

$$\nabla^2 V_a(i, j) = rI(i, j) \tag{1}$$

where ∇^2 is the laplacian operator as shown in Eq. (2).

$$\begin{aligned}\nabla^2 V_a(i, j) = {} & V_a(i-1, j) + V_a(i+1, j) \\ & + V_a(i, j-1) + V_a(i, j+1) - 4V_a(i, j)\end{aligned} \tag{2}$$

An equation similar to Eq. (1) is obtained for layer B using the same method described above.

$$\nabla^2 V_b(i, j) = -rI(i, j) \tag{3}$$

B. Tactile element position coordinates

The position $x_{i,j}$ of each element along the x direction is defined. This $x_{i,j}$ is a function of j only and is taken as an arithmetic series in the direction of j. $x_{i,j}$ is determined from Eq. (4) defining the origin which falls at the center of the sensor.

$$x_{i,j} = \frac{2j - (n+1)}{n-1} \tag{4}$$

Eq. (5) is obtained similar to Eq. (4) as follows;

$$y_{i,j} = \frac{-2i + m + 1}{m-1} \tag{5}$$

Since the tactile elements are arranged at equal intervals, $x_{i,j}, y_{i,j}$ for the tactile elements becomes an arithmetic progression resulting to the following equation.

$$\nabla^2 x_{i,j} = \nabla^2 y_{i,j} = 0 \tag{6}$$

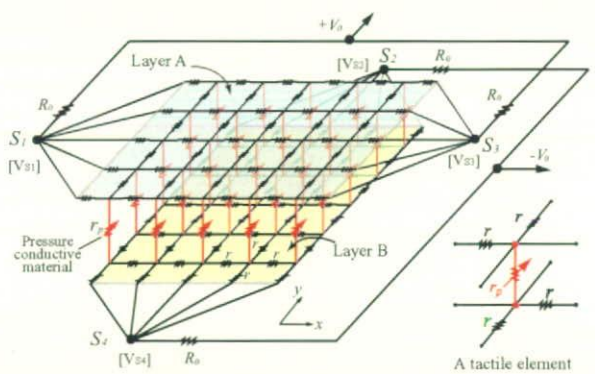

Fig. 2. Structure of the sensor

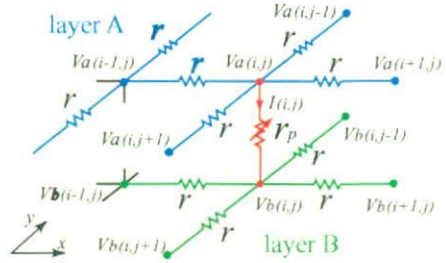

Fig. 3. Equivalent circuit of the sensor

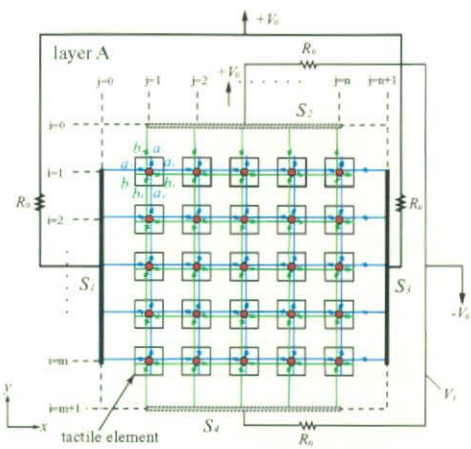

Fig. 4. Connection of tactile elements in layer A

C. Boundary conditions

Let us consider the boundary condition about layer A. Boundaries S_2 and S_4 are not connected anywhere so that and S_2 and S_4 are open terminals. Therefore it become as follows;

$$V_a(0, j) = V_a(1, j), \quad V_a(m+1, j) = V_a(m, j) \tag{7}$$

Concidering boundaries S_1 and S_3 , there are tactile elements of layer A that are connected to the electrodes E_1 and E_3 so that currents flows in from the electrodes. Since the total of these currents is equal to the currents which flows through R_0, the boundary conditions are determined from Eq. (8), (9).

$$\frac{1}{R_0}\Big\{V_0 - V_{E1}\Big\} = \frac{1}{r}\Big\{\sum_{i=1}^{m}\Big(V_{E1} - V_a(i, 1)\Big)\Big\} \tag{8}$$

$$\frac{1}{R_0}\Big\{V_0 - V_{E3}\Big\} = \frac{1}{r}\Big\{\sum_{i=1}^{m}\Big(V_{E3} - V_a(i, n)\Big)\Big\} \tag{9}$$

Moreover, since for the electrode E_1 is $j = 0$, and for E_3 is $j = n + 1$ in the sensor, then the boundary condition becomes;

$$V_a(i, 0) = V_{E_1}, \quad V_a(i, n+1) = V_{E_3} \tag{10}$$

Using the same methods described above for layer B, equations similar to Eq. (7), (8), (9) and (10) are obtained.

D. First-order moments of the current density distribution

The center position of the current distribution is determined by computing the first-order moments of the current distribution with respect to the x-axis. When the pressure-sensitive element is arranged in the shape of a matrix $m \times n$, the first-order moments of current distribution is expressed;

$$I_x = \sum_{i=1}^{m}\sum_{j=1}^{n} x_{i,j} I(i,j) \tag{11}$$

Considering I_x, Eq. (1) is applied to Eq. (11), resulting to;

$$I_x = \frac{1}{r}\sum_{i=1}^{m}\sum_{j=1}^{n} x_{i,j}\nabla^2 V_a(i,j) \tag{12}$$

Substituting Eq.(2) for Eq.(12) gives Eq. (13). Rearranging Eq. (13) gives Eq. (14).

$$\begin{aligned} I_x &= \frac{1}{r}\sum_{i=1}^{m}\sum_{j=1}^{n} x_{i,j}\nabla^2 V_a(i,j) \\ &= \frac{1}{r}\left\{\sum_{i=1}^{m}\sum_{j=1}^{n} x_{i,j}V_a(i-1,j) + \sum_{i=1}^{m}\sum_{j=1}^{n} x_{i,j}V_a(i+1,j)\right. \\ &\quad + \sum_{i=1}^{m}\sum_{j=1}^{n} x_{i,j}V_a(i,j-1) + \sum_{i=1}^{m}\sum_{j=1}^{n} x_{i,j}V_a(i,j+1) \\ &\quad \left. -4\sum_{i=1}^{m}\sum_{j=1}^{n} x_{i,j}V_a(i,j)\right\} \end{aligned} \tag{13}$$

$$\begin{aligned} I_x = \frac{1}{r}\Big\{&\sum_{i=1}^{m}\sum_{j=1}^{n} V_a(i,j)\nabla^2 x_{i,j} \\ &+ \sum_{j=1}^{n}\Big(x_{m,j}V_a(m+1,j) - x_{m+1,j}V_a(m,j)\Big) \\ &+ \sum_{j=1}^{n}\Big(x_{1,j}V_a(0,j) - x_{0,j}V_a(1,j)\Big) \\ &+ \sum_{i=1}^{m}\Big(x_{i,n}V_a(i,n+1) - x_{i,n+1}V_a(i,n)\Big) \\ &+ \sum_{i=1}^{m}\Big(x_{i,1}V_a(i,0) - x_{i,0}V_a(i,1)\Big)\Big\} \end{aligned} \tag{14}$$

Since $x_{i,j}$ is equal to the direction of i, and also using Eq.(6), Eq.(7), the 1st, 2nd and 3rd term of Eq.(14) reduced to zero. Thus Eq. (14) is simplified as follows;

$$\begin{aligned} I_x = \frac{1}{r}\Big\{&\sum_{i=1}^{n}\Big(x_{i,n}V_a(i,n+1) - x_{i,n+1}V_a(i,n)\Big) \\ &+ \sum_{i=1}^{n}\Big(x_{i,1}V_a(i,0) - x_{i,0}V_a(i,1)\Big)\Big\} \end{aligned} \tag{15}$$

When the boundary conditions Eq. (8) and Eq.(9), are applied to Eq. (15), and using Eq.(10), Eq.(15) is simplified to Eq. (16);

$$I_x = \frac{1}{n-1}\left(\frac{2m}{r} + \frac{n+1}{R_0}\right)\cdot(V_{E_1} - V_{E_3}) \tag{16}$$

Similarly, the first-order moments of the current distribution with respect to the y direction is determined as follows.

$$I_y = \frac{1}{m-1}\left(\frac{2n}{r} + \frac{m+1}{R_0}\right)\cdot(V_{E_2} - V_{E_4}) \tag{17}$$

The total current is calculated from the sum of the currents following into the electrodes E_1 and E_3 through resistance R_0 as shown in Eq.(18). The total current folowing through electrodes E_2 and E_4 are computed likiwise.

$$I_{all} = \sum_{i=1}^{m}\sum_{j=1}^{n} I(i,j) \tag{18}$$

$$= \frac{2V_0 - V_{E_1} - V_{E_3}}{R_0} \quad = \frac{2V_0 + V_{E_2} + V_{E_4}}{R_0} \tag{19}$$

From the above equations, the center position of current distribution is calculated from Eq.(20)

$$x_0 = (I_x)/(I_{all}), \quad y_0 = (I_y)/(I_{all}) \tag{20}$$

E. Measurement of the center of the pressure distribution

The purpose of the proposed sensor is to measure the center of the pressure distribution. Therefore, let us consider the relationship between the current density $i(x,y)$ and the distributed load $F(i,j)$. A pressure-sensitive electro-conductive rubber is used as a load sensing element. Its resistance r_p changes with load $F(i,j)$. The relation between resistance and load is represented by Eq. (21)

$$r_p(i,j) = \frac{1}{f(F(i,j))} \tag{21}$$

Since the resistance r is much lower than the resistance r_p, $(r_p \gg r)$, the voltage of layers A and B may be considered to be approximately constant. Thus, the following relationship is obtained:

$$\begin{aligned} I(i,j) = \frac{V_a(i,j) - V_b(i,j)}{r_p(i,j)} &= \frac{V_a - V_b}{r_p(i,j)} \\ &= (V_a - V_b)f(F(i,j)) \end{aligned} \tag{22}$$

The relation between resistance and load is assumed to follow Eq. (23), where resistance is in inverse proportion to the load.

$$r_p = \frac{1}{f(F)} = kF^{-1} \tag{23}$$

k in the equation is a constant. The center position of the load distribution x_0,y_0 and the total distributed load are then determined from the following equations.

$$x_0 = \frac{\sum_{i=1}^{m}\sum_{j=1}^{n} x_{i,j}\cdot F(i,j)}{\sum_{i=1}^{m}\sum_{j=1}^{n} F(i,j)} = \frac{I_x}{I_{all}} \quad (24)$$

$$y_0 = \frac{\sum_{i=1}^{m}\sum_{j=1}^{n} y_{i,j}\cdot F(i,j)}{\sum_{i=1}^{m}\sum_{j=1}^{n} F(i,j)} = \frac{I_y}{I_{all}} \quad (25)$$

$$F_t = \sum_{i=1}^{m}\sum_{j=1}^{n} F(i,j) = \frac{kI_{all}}{(V_a - V_b)} \quad (26)$$

IV. Placement of Tactile Elements

As described previously, the tactile elements are consist of resistors and a pressure-sensitive material. These tactile elements are arranged in a matrix, as shown in Fig. 5(a). However, a structure without any pressure-sensitive material, is also possible, in which case, the resistance of the pressure-sensitive material is equivalent to infinity.

In structures that do not include any pressure-sensitive material, tactile elements consist of resisters only, so that the strucrure are extremely compact. Accordingly, this increases flexibility in placement options, as shown in Fig. 5(b).

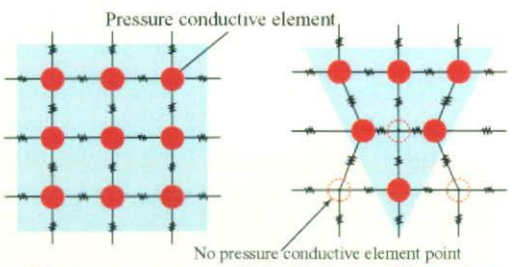

(a) Basic arrangement (b) Application to arbitrary shape

Fig. 5. Arrangement method of tactile element

V. Prototype of Sensor

The initial prototype sensor used a pressure-conductive rubber (dimensions $12mm \times 12mm \times 5.2mm$ thick) manufactured by Inaba rubber CO.LTD, as the pressure-sensitive material. The prototyped sensor is shown in Fig.6. The elements were arranged in a 3×3 grid. The resistance value was $r = 150\Omega$. As the sensor has a net-structure, it can be mounted on the sphere as shown in Fig. 6(b).

VI. Experimental Validation of Characteristics

The sensor is disigned to measure the overall load and the central position of the load distribution. To experimentally verify these basic functionalities of the sensor, load-measuring experiments and position-measuring experiments were conducted. As shown in Fig.8(a) , each tactile element was numbered from $T(1,1)$ through to $T(3,3)$.

A. Load-measuring experiment

In this experiment, cycle of pressure was applied to the central tactile element of the sensor $T(2,2)$ at a frequency of 0.2Hz using a vibrator(Wilcoxon research, F4/Z820WA), the tip of which was fitted with a load cell. The load cell output

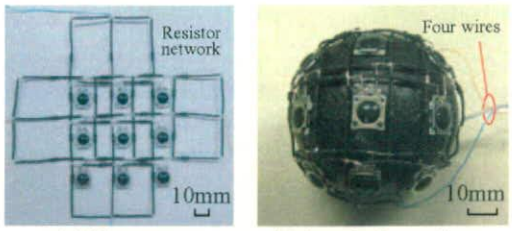

(a) The sensor (b) Attached on sphere

Fig. 6. Initial prototype of the net structure tactile sensor.

and the overall load output were measured. The results of this experiment are shown in Fig.7. A difference in output value due to the influence of hysteresis of the pressure-conductive rubber was observed when pressure was increased or decreased.

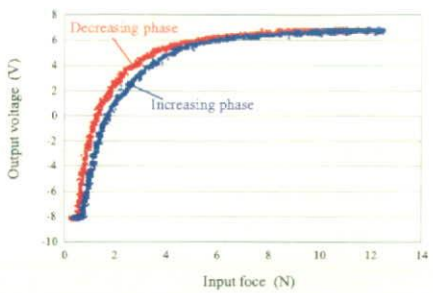

Fig. 7. Experimental result of sensor's total load output

B. Position-measuring experiment

When a load is applied to a single point, the sensor outputs the position where the load is applied. When loads are applied to multiple points, the sensor outputs the center position where the multiple points are applied.

1) Position-measuring experiment for a single-point: In this experiment, a load was applied to a single point on tactile element and the sensor position output value was measured. Fig.8(b) shows sensor's output (v_x,v_y) when load was applied to each element. It was observed that the output's position was very well in agreement with the point of application of the load. The x component and the y component of the sensor's output changed at $3V$ intervals.

2) Position-measuring experiment when loads are applied to two points: In this experiment, loads were applied to two points. A constant load of 3N was applied to the tactile element at $T(2,3)$, while a load ranging from 0N to 3N was applied to the tactile element at point $T(2,1)$. The results of this experiment are shown in Fig.9. It was observed that sensor output changed proportionally with the load applied to the tactile element at $T(2,1)$. It can be seen here that when the load applied to $T(2,1)$ was at 3N, the sensor output value was $0V$, its means the load distribution was centered.

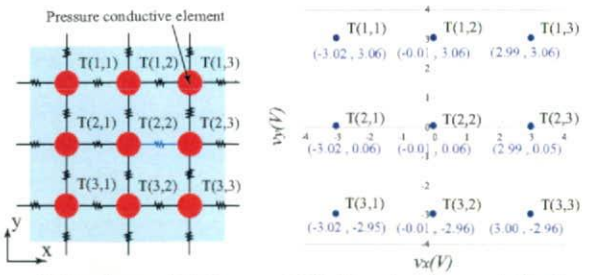

(a) Traial sensor for test (b) Position output for one point loading

Fig. 8. Experimental results of sensor's position output for one point loading

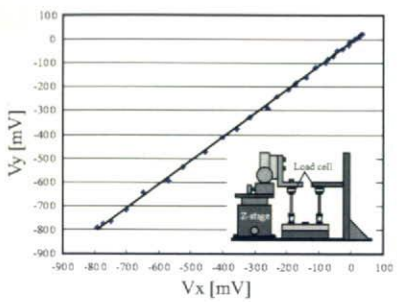

Fig. 9. Experimental results of sensor's position output for two point loading

C. Position output when an impact load is applied (response time)

An experiment was carried out to clarify the response time of the sensor. In this experiment, an impact load was applied to the sensor using an impulse hammer (Ono sokki, GK-300), and the time until the position output value of the sensor became stable was measured. The experimental result is shown in Fig. 10. The time after adding the impact load until the value of the impact position becomes stable is approximately $0.6ms$. Generally, controlling a robot using sensor feedback requires the control cycle time to be within $1ms$. Thus, the proposed sensor can be used for such an application. The delay in the response time of the sensor is primarily a result of the delay in the response of the pressure-conductive rubber.

VII. Covering

When tactile elements are placed discretely, the load distribution between each element becomes a problem. For example, any load applied between each element cannot be detected. Accordingly, after each element is put in place, the elements must be covered with a flexible material such as silicon rubber. When each tactile element is covered with silicon rubber, any load applied to this cover also applies to the tactile element beneath as indicated by Eq. (27).

$$s(x,y) = \iint g(\xi,\eta) f(x-\xi, y-\eta)\, d\xi d\eta \qquad (27)$$

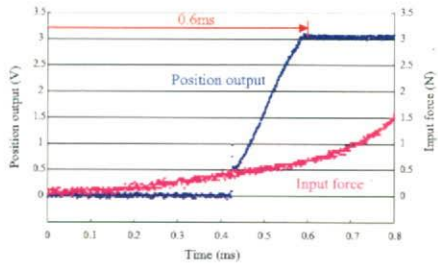

Fig. 10. Time response of the sensor'position output with an impulse load.

here, $f(x,y)$ is a load applied on the cover, $s(x,y)$ is pressure distribution on the tactile element, $g(x,y)$ is the pressure distribution under the cover on whose surfase point load $F\cdot\delta(0,0)$ is applied[13]. Thus, the load is spread among the individual elements. This is how the sensor is able to output the central point and the overall load. As shown in Fig.11(a), the sensor used in the experiments is covered with a hemispherical styrene foam. When the top surface of the cover was stroked with a finger to drawn a circle, the locus of the position output of the sensor was shown in the Fig.11(b).

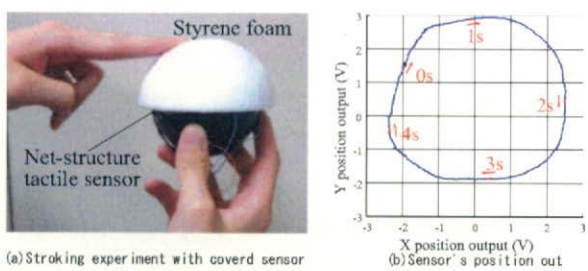

(a) Stroking experiment with coverd sensor (b) Sensor's position out

Fig. 11. Stroking experiment with sensor covered by styrene foam.

VIII. Prototype of Tactile Element

A prototype tactile element was constructed. As shown in Fig.12, the sensor was formed of a resistor network combined with pressure-sensitive elements. The pressure-sensitive elements consist of pressure-conductive rubber laid down on top of electrodes (spiral shape). When load is applied to the rubber, the resistance of the rubber decreases, and the change in resistance value is measured by the spiral electrodes. The resistors used were chip-resistor.

Fig.13 shows the prototype of the tactile elements, arranded on a 3×3 matrix form. The tactile element's dimensions were $10mm$ per side by $1mm$ thick. Each element can be cut from the sheet and may be attachable on any surface. Fig.fig:HokouSensorPart shows tactile sensor arranged to 25×5 grid as the example. In this example, the area of sensor was extended and this sensor was used for walk measurement [16]. It was confirmed to operate appropriately when there ware many wire like this example.

IX. Summary

A prototype net-structure tactile sensor was constructed with the aim of developing a sensor capable of covering a

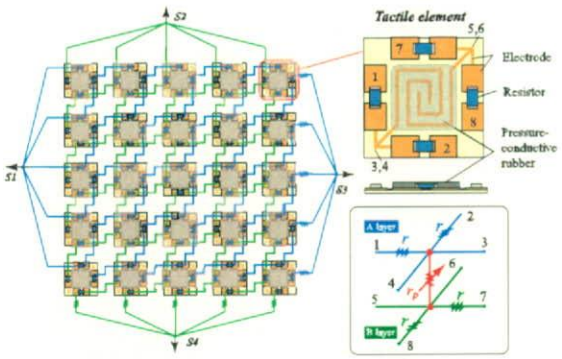

Fig. 12. Sensor using prototype of tactile element an enlarged view of tactile element

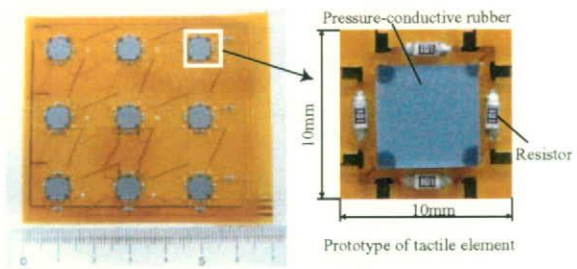

Fig. 13. Prototype of tactile element arranded on 3×3 grid. Each element can be cut from the sheet and may be attachable on any surface.

robot's entire structure, including freeform surfaces, while reducing wiring requirement and ensuring high-speed response. The sensor is net-structured, capable of mounted on freeform surfaces, and can detect overall load, as well as the central point of load distribution, on 2-dimensional surfaces. The wiring requirement for multiple detection elements is simplified with only 4 output wires from the sensor. Moreover, the sensor response speed is nearly constant, regardless of the number of detection elements, their placements, or sensor areas. In this paper, the principle of the sensor, the process of constructing the prototype and the results of experiments were described.

X. ACKNOWLEDGMENTS

We wish to express our thanks to Inaba rubber CO.,LTD for providing us with the protype of the tactile element.

REFERENCES

[1] H.R.Nicholls, M.H.Lee," *Int.J. Robotics Research*, vol.8, no.3, pp.3-30,1989.
[2] M.H.Lee, H.R.Nicholls, "Tactile Sensing for Mechatronics- A State of the Art Survey," *Mechatronics*, Vol.9, pp.1-31, 1999.
[3] M.Inaba, Y.Hoshino,K.Nagasaka,T.Ninomiya, S.Kagami, H.Inoue, "A Full-Body Tactile Sensor Suit Using Electrically Conductive Fabric and Strings," *Pro. the IEEE/RSJ Int. Conf.Intelligent Robots and Systems*, pp. 450-457, 1996.
[4] T.V. Papakostas, J.Lima, M. Lowe, "A large area force sensor for smart skin applications," *Proc. Int. Conf. on Sensors*, pp.1620-1624, 2002.
[5] T. Mukai, "Soft Areal Tactile Sensors with Embedded Semiconductor Pressure Sensors in a Structured Elastic Body," *Proc. IEEE Sensors*, pp.1518-1521, 2004

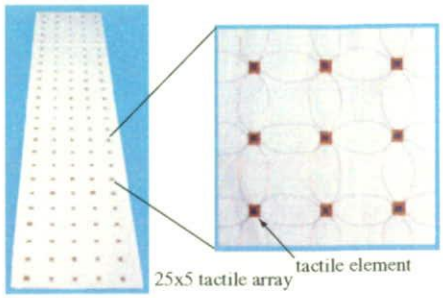

Fig. 14. Part of tactaile element arranded on 25×5 grid. Each element is cut from the sheet.

[6] Y. Ohmura, Y. Kuniyoshi, A. Nagakubo, "Conformable and Scalable Tactile Sensor Skin for Curved Surfaces," *Proc. IEEE Int. Conf. on Robotics and Automation*, pp.1348-1353, 2006
[7] M. Hakozaki, H. Oasa and H. Shinoda, "Telemetric Robot Skin," *Proc. IEEE Int. Conf. on Robotics and Automation*, pp.957-961,1999.
[8] M. Nilsson, "Tactile Sensors and Other Distributed Sensors with Minimal Wiring Complexity," *IEEE/ASME Trans. Mechatronics*, Vol.5, No.3, pp.253-257, 2000.
[9] S. Ando, H. Shinoda, A. Yonenaga, and J. Terao,Ultrasonic, "Six-Axis Deformation Sensing," *IEEE trans. on ultrasonics, ferroelectrics, and frequency control*, Vol. 48, no. 4, pp.1031-1045, 2001.
[10] M. Ohka, H. Kobayashi, Y. Mitsuya, "Sensing characteristics of an optical three-axis tactile sensor mounted on a multi-fingered robotic hand," *IEEE/RSJ Int. Con. on Intelligent Robots and Systems*, pp.493-498, 2005
[11] K.Kamiyama, K. Vlack,T. Mizota, H. Kajimoto, K. Kawakami,S. Tachi, S., "Vision-based sensor for real-time measuring of surface traction fields," *IEEE Computer Graphics and Applications*, Vol.25, no.1, pp.68-75, 2005.
[12] K. Noda, K. Hoshino, K. Matsumoto, I. Shimoyama, "A shear stress sensor for tactile sensing with the piezoresistive cantilever standing in elastic material," *Sensors and Actuators A*, 127,pp.295-301,2006.
[13] M.Shimojo, "Mechanical Filtering Effect of Elastic Cover for Tactile Sensor," *IEEE Trans. Robotics and Automation*, Vol.13, no.1, pp.128-132,1997.
[14] M.Ishikawa "A method for measuring the center position and the total intensity of an output distribution of matrix positioned sensors," *Trans. SICE*, Vol.19, no.5,pp.381-386,1983.
[15] M.Shimojo T.Araki A.Ming M.Ishikawa, "A ZMP Sensor for a Biped Robot," *Proc. IEEE Int. Conf. Robotics and Automation*, 2005.
[16] M.Hirasawa K.Katano H.okada M.Shimojo, "Development of a Walking Position Sensor for Wide Range Gait," *SICE SI2007*,p513-514 2007.